Condition Parameter Estimation for Buck Converters based on Model Observers

Zhaohui Cen and Paul Stewart (Senior Member IEEE)

***Abstract*—DC-DC power converters such as Buck converters are susceptible to degradation and failure due to operating under conditions of electrical stress and variable power sources in power conversion applications such as electric vehicles and renewable energy. Some key components such as electrolytic capacitors degrade over time due to evaporation of the electrolyte. In this paper, a model-observer based scheme is proposed to monitor states of Buck converters and to estimate their component parameters such as capacitance and inductance. Firstly, a diagnosis observer is proposed, and the generated residual vectors are applied for fault detection and isolation. Secondly, component condition parameters such as capacitance and inductance are reconstructed using another novel observer with adaptive feedback law. Additionally, the observer structures and their theoretical availability are analyzed and proven. In contrast to existing reliability approaches applied in Buck converters, the proposed scheme perform online-estimation for key parameters. Finally, Buck converters in conventional DC-DC step-down and Photo-Voltaic applications are investigated to test and validate the effectiveness of the proposed scheme in both simulation and laboratory experiment. Results demonstrate the feasibility, performance and superiority of the proposed component parameters estimation scheme.**

***Index Terms*—Buck converters, condition monitoring and fault diagnosis, model observers, adaptive estimation**

I. Introduction

As a key power systems component, power converters have important functions such as DC-DC conversions and DC-AC inversions to feed power into local loads or power grids. However, the power converters are also subject to degradation and ageing, which is exacerbated by running under uninterrupted operating regimes and unstable or unsteady power inputs in conventional power systems, typically in the applications areas of, for example, electric vehicles(EV), wind energy conversion systems, photo-voltaic(PV) systems and smart-grid systems [1]–[9]. Also, mismatches among different PV modules often occur, when modules in an array do not exhibit fully identical electrical properties , or they are exposed to arid environmental conditions such as strong irradiance, high levels of airborne dust particles and high temperatures, often leading to a different maximum power point (MPP) for each module. Furthermore, If PV modules are installed in strings, the string systems will lower the string's output to the level of the lowest performing module, due to the unbalance of PV cells caused by power electronics performance degradation [10]. Therefore, it is essential to monitor conditions of the PV module-level power converters and to further estimate the degradation status in real-time or in advance to avoid fatal failures and improve the reliability of the overall power system.

Currently, most reliability studies on power converters and power systems are focused on fault mechanism analysis, characteristic signal analysis and qualitative fault mode identification because of limited measurable state signals [11]–[17]. The possible faulty components involved in power electronics are shown in Fig. 1 [18], [19]. The left pie chart in Fig. 1 shows that capacitors are the most vulnerable components. Also, the semiconductor components such as MOSFETs and IGBTs have a large proportion of failure distributions [20]. Based on these failure and fault types in power electronics, some diagnostic techniques focus on converter terminal quantities such as output voltage frequency analysis and motor stator current time-domain response. The current vector trajectory in the Concordia frame [21]–[24], has been adopted to identify faulty components, and detect and diagnosis converter failures at system level [25]. However, because these approaches utilize off-line signals or periodic duration signals, they are not real-time, which generally depends on complicated artificial fault analysis. In addition, some real-time diagnostic techniques based on voltages or currents of power electronics devices were studied in [26], [27], but they are only applicable to faults of switch components such as IGBTs and MOSFETs. [28]–[30] studied fault diagnosis of power inverters based on artificial intelligence and data-driven methods such as artificial neural networks (NN). These approaches are able to diagnosis typical component faults based on the measured voltage and current signals. However, they are only applicable for specified faults and device conditions. Also, because the NN needs to be trained first based on its sample data from the historical fault-free and faulty signal, the diagnosis efficiency closely depends on the diversity of sample date signals.

Although most studies described above focus on fault mechanism analysis and qualitative diagnosis of power converters, few quantitative approaches are proposed to monitor the states of the power converter and its components in real-time. Conventionally, the components such as capacitors and inductors can be off-line measured and detected based on LCR metering devices. However, the LCR metering measurement is not executed in real-time, limiting its applicability for online reliability monitoring and feedback control in real-time. Also, it is a challenge to estimate C and L based on online signals because

Zhaohui Cen is with xxxx, xxxx, xxx, e-mail: xxxx.

Paul Stewart is with the Institute For Innovation in Sustainable Engineering, University of Derby, UK.

Manuscript received xxx xx, 2015; revised xxx xx, 2015.

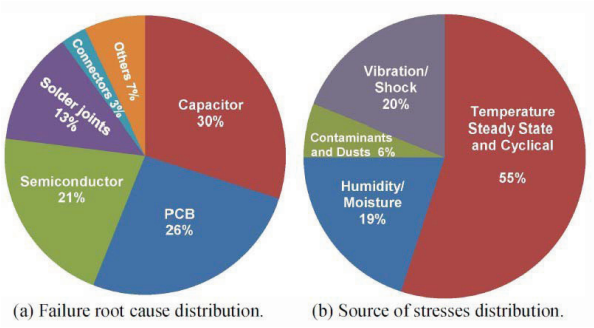

Fig. 1. Failure and stress distributions in power electronics systems. [18], [19]

both the circuit dynamics and diversity of time-varying signals is complex. In order to address the challenge for online monitoring, a model-based fault detection approach was proposed in [31], [32], but the studied models do not correlate well with transient behaviors of power electronics. [33]–[36] proposed a model observer for Buck converters and inverters, which can detect and isolate components fault in real-time. However, all the published quantitative works are not able to accomplish a high-level and real-time accurate Condition Parameter Estimation (CPE), which can indicate condition factors of components in power electronics.

Compared to studies mentioned above, the main contribution of this paper is to demonstrate monitoring and estimation of the condition parameters of power converters in real-time. Residual vectors generated from the proposed model observer are applicable for fault detection and isolation. Additionally the component condition parameters can be reconstructed based on the observer adaptive feedback law, which can estimate unknown states and parameters based on limited measurable states. Unlike former reliability approaches applied in power electronics, it can not only monitor the condition of power converters in real-time, but also estimate the parameters of its components. This capability is useful for isolating the faulty components of power systems and improving the reliability and efficiency of PV system with grid integration.

This paper is organized as follows. In Section II, the mathematical model of a buck power converter and problem formulation are elaborated. Section III presents the model observers with an adaptive law for condition parameters estimation. Section IV shows the simulation results obtained for various fault components and fault scenarios when the proposed scheme works for the buck power converter. A conventional buck converter hardware setup and experimental results for inductance and capacitance estimation are presented in Section V. Validation for Buck converters under PV MPP Tracking(MPPT) control is investigated in Section VI. Finally, a conclusion is provided in Section VII.

II. Model Framework and Problem Formulation

Because of its representativeness and popularity in PV power systems, a single-phase DC-DC buck converter in Fig. 2 is considered to build the model and hardware in this paper, subsequently the CPE problem is formulated and defined.

A. Single-phase buck converter with resistor load

Considering the single-phase DC-DC power converter in Fig. 2 and Fig. 3, it is comprised of a semiconductor switch Q, an inductor L, a capacitor C, a diode D and a resistor Load R. The basic operation of the buck converter is controlling the inductor current by two switches (the transistor Q and the diode D). The conceptual model of the buck converter is best understood in terms of the relation between current and voltage of the inductor. Therefore, a power electronics converter can be thought of as a switched system, i.e., a continuous-time system with discrete (isolated) switching events, and (in general), its dynamics can be described by a linear-switched state-space model of the form.

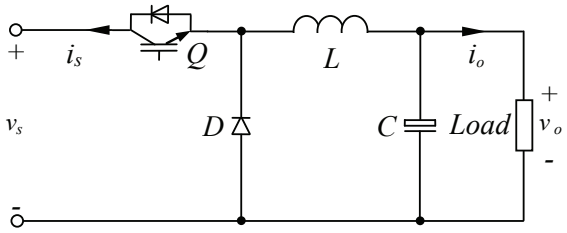

Fig. 2. Topology of Buck converter.

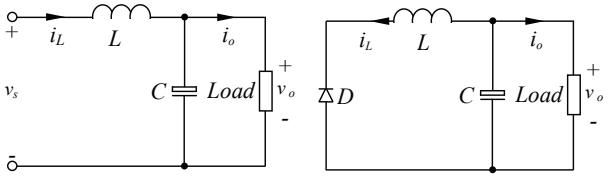

Fig. 3. Buck converter in charging Mode (left) and Buck converter in discharging (right).

The nominal (Pre-Fault) system state-space model of the buck converter can be denoted as:

$$\begin{bmatrix} \dot{I}_L \\ \dot{U}_o \end{bmatrix} = \begin{bmatrix} 0 & -\frac{1}{L} \\ \frac{1}{C} & -\frac{1}{RC} \end{bmatrix} \begin{bmatrix} I_L \\ U_o \end{bmatrix} + \begin{bmatrix} \sigma(t)/L \\ 0 \end{bmatrix} U_i \tag{1}$$

$$\begin{bmatrix} I_L^m \\ U_o^m \end{bmatrix} = \begin{bmatrix} 1 & 0 \\ 0 & 1 \end{bmatrix} \begin{bmatrix} I_L \\ U_o \end{bmatrix} \tag{2}$$

where L is the inductance of the inductor, C is the capacitance of the capacitor, R is the load resistance. $\sigma : [0, \infty) \rightarrow \{0, 1\}$ is the binary switching signal governing the Switch Q. the description in (2) can be completed with

$$y = \begin{bmatrix} I_L^m & U_o^m \end{bmatrix}^T = C' x \tag{3}$$

where $C^{'} = I_{2\times2}, x = [I_L, U_o]^{'}$ and the superscript m denotes measurement value, describing the measurements available to the controller. Also, (1) and (2) can be denoted as the standard format of state-space model $\dot{x} = Ax + Bu$, where

$$A = \begin{bmatrix} 0 & -\frac{1}{L} \\ \frac{1}{C} & -\frac{1}{RC} \end{bmatrix}, B = \begin{bmatrix} \sigma(t)/L \\ 0 \end{bmatrix}, u = U_i \tag{4}$$

If a fault or parameter variation has occurred in the system, these factors will cause a change in the matrices of any or all subsystems in (1) and (2). Without loss of generality, faults in the inductor L and the output filter capacitor C are considered. The faults may cause the inductor or the capacitor to degrade slowly over time, which would result in a gradual decrease of inductance or capacitance (soft fault), or it may cause a sudden failure open or short (hard fault). Thus, the variation caused by faults can be denoted as $\tilde{A} = A + \Delta A$ and $\tilde{B} = B + \Delta B$. Also, the condition parameters of the buck converter can be denoted as $\theta = \begin{bmatrix} L & C \end{bmatrix}^{'}$. Consequently, the post-fault system Model can be described by

$$\begin{bmatrix} \dot{I}_L \\ \dot{U}_o \end{bmatrix} = \begin{bmatrix} 0 & -\frac{1}{L+\Delta L} \\ \frac{1}{C+\Delta C} & -\frac{1}{R(C+\Delta C)} \end{bmatrix} \begin{bmatrix} I_L \\ U_o \end{bmatrix} + \begin{bmatrix} \sigma(t)/(L+\Delta L) \\ 0 \end{bmatrix} U_i \tag{5}$$

It can also described in the format of state-space model as

$$\begin{aligned} \dot{x} &= (A + \Delta A)x + (B + \Delta B)u \\ y &= C^{'}x \end{aligned} \tag{6}$$

B. Condition parameter estimation problem formulation

Considering (6), the condition parameter estimation problem consists of designing a detection filter that takes u and y as inputs and generates a residual vector with the following properties: i) when there is no fault, the residual is identical to zero, and ii) when a fault occurs, the residual is clear enough to differentiate between different faults from the capacitor, inductor, and switch. iii) If the soft faults of capacitors and inductors occur, the condition parameters $\theta = \begin{bmatrix} L & C \end{bmatrix}^{'}$ can be estimated for condition monitoring.

III. Fault diagnosis and condition monitoring using model observer

In this section, a fault diagnosis and condition monitoring scheme comprised of a module of the fault diagnosis observer and corresponding modules of parameter estimation observers is proposed. Firstly, the fault is detected and isolated by the fault diagnosis observer. Secondly, the corresponding parameter estimation observer module is triggered by the FDI result. The overall scheme process can be seen in Fig. 4.

A. Fault diagnosis observer

Following the notation of section 2, a fault diagnosis observer for the system in Fig. 2 is given by

$$\begin{bmatrix} \dot{\hat{I}}_L \\ \dot{\hat{U}}_o \end{bmatrix} = \begin{bmatrix} 0 & -\frac{1}{L} \\ \frac{1}{C} & -\frac{1}{RC} \end{bmatrix} \begin{bmatrix} \hat{I}_L \\ \hat{U}_o \end{bmatrix} + \begin{bmatrix} \sigma(t)/L \\ 0 \end{bmatrix} U_i + K\left(y - C^{'} \begin{bmatrix} \hat{I}_L \\ \hat{U}_o \end{bmatrix} \right) \tag{7}$$

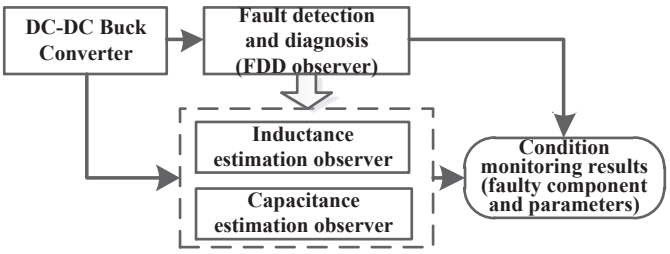

Fig. 4. Fault diagnosis and condition parameter estimation scheme.

where $\sigma(t)$, U_i, y are same as in (1), and the third term in the right side is feedback of observer with gain K, which works to keep the observer states tracking the real states. Also, (7) can be represented as

$$\begin{aligned} \dot{\hat{x}} &= A\hat{x} + Bu + K(y - \hat{y}) \\ \hat{y} &= C^{'}\hat{x} \end{aligned} \tag{8}$$

Although $C^{'} = I_{2\times2}$ and the system of (1) has a full rank, the system is only theoretically observable when $\sigma(t) = 1$, otherwise it is not observable. In order to guarantee that the observability property is preserved, it is necessary to consider $\sigma(t)$ as a regularly persistent input . Consequently, the error dynamics $e = x - \hat{x}$ can be defined as

$$\dot{e} = (A - KC)e \tag{9}$$

A further theorem based on analysis above is given as follows:

Theorem 1. *If there exists a certain symmetric positive definite matrix $P \in \mathbb{R}^{2\times2}, P = P^T$ and some $\rho \in \mathbb{R}_{>0}$, the Linear Matrix Inequality (LMI) below is satisfied as*

$$(A - KC)^T P + P(A - KC) < -\rho P \tag{10}$$

Then the error dynamics (9) *are globally asymptotically stable.*

The proof of Theorem 1 can be referred to Theorem 4.4 in [31]. The solution of the inequality (10) can be obtained from the following Theorem 2.

Theorem 2. *If there exists a certain symmetric positive definite matrix $P \in \mathbb{R}^{2\times2}, P = P^T$ and some $\rho \in \mathbb{R}_{>0}$, the LMI below is satisfied as*

$$(PA - YC)^T + (PA - YC) < -\rho P \tag{11}$$

Then the inequality (10) is satisfied with P and by taking $L = P^{-1}Y$.

The proof of Theorem 2 can be referred to Lemma 4.5 in [31].

Remark: based on the residuals $e = x - \hat{x}$ generated by the fault diagnosis observer, fault detection and fault isolation can be implemented based on the time-domain property of the residual signal, which is further demonstrated in section IV.

B. Inductance estimation for the inductor

If a fault for the inductor is detected and isolated by the fault diagnosis observer, an inductance estimation observer is triggered to estimate the accurate value of inductance offset. Denoting the estimation errors as $\tilde{x} = \hat{x} - x$ and $\tilde{L} = \hat{L} - L$, the observer is designed as follows.

$$\begin{aligned} \dot{\hat{x}} &= A\big(C,\hat{L}\big)\hat{x} + B\big(C,\hat{L}\big)u + K(y-\hat{y}) \\ \hat{y} &= C^{'}\hat{x} \end{aligned} \tag{12}$$

Denoting the matrices errors as

$$\begin{aligned} A\big(C,\hat{L}\big) - A(C,L) &= f_A(\frac{\delta A}{\delta L},\tilde{L}) \\ B\big(C,\hat{L}\big) - B(C,L) &= f_B(\frac{\delta B}{\delta L},\tilde{L}) \end{aligned} \tag{13}$$

We also can denote (12) as

$$\begin{aligned} \dot{\hat{x}} &= A(C,L)\hat{x} + f_A(\frac{\delta A}{\delta L},\tilde{L})\hat{x} + B(C,\hat{L})u + K(y-\hat{y}) \\ \hat{y} &= C^{'}\hat{x} \\ \dot{\hat{L}} &= \Gamma_L G\big(y-\hat{y}\big) \end{aligned} \tag{14}$$

The error dynamics are described by

$$\begin{aligned} \dot{\tilde{x}} &= (A-KC)\,\tilde{x} + F \\ F &= f_A(\frac{\delta A}{\delta L},\tilde{L})\hat{x} + f_B(\frac{\delta B}{\delta L},\tilde{L})u \end{aligned} \tag{15}$$

A further theorem on how to obtain τ_L above is given below.

Theorem 3. *With the observer gain K in Theorem 1 and a defined matrix $Q_{(2\times 2)} > 0$, and positive parameter Γ_L , if there exists two matrices $P_{2\times 2}$ and $G_{2\times 2}$ satisfying*

$$\begin{aligned} P(A-KC) + (A-KC)^T P + \Gamma_L P &= -Q \\ PB &= C^T G^T \end{aligned} \tag{16}$$

Then the observer given in (12) *with the adaptive fault estimation law as follows:*

$$\dot{\hat{L}} = \Gamma_L G\big(y-\hat{y}\big) \tag{17}$$

can lead to $\lim_{t\to\infty}\tilde{x}(t) = 0$ *and* $\lim_{t\to\infty}\tilde{L}(t) = 0$, *where* Γ_L *is a positive constant value.*

Proof. Set $\eta(t) = x(t) - \Theta\tilde{L}(t)$ and $\Xi(\tilde{L}) = (A-KC)\Theta\tilde{L} + F(\tilde{L})$. For writing convenience and as long as there is no ambiguity, the time derivable t shall be omitted in the sequel. From (15) One can get

$$\dot{\eta} = (A-KC)\eta + (A-KC)\Theta\tilde{L} + F(\tilde{L}) \tag{18}$$

Set $V_1 = \eta^T P\eta$ and $V_2 = \tilde{L}^T\Gamma_L^{-1}\tilde{L}$ where P is given in (16) and Γ_L^{-1} is given in (17). Let $V = V_1 + V_2$ be a Lyapunov candidate function. One can obtain

$$\begin{aligned} \dot{V}_1 &= \dot{\eta}^T P\eta + \eta^T P\dot{\eta} \\ &\doteq \eta^T\big[(A-KC)^T P + P(A-KC)\big]\eta + 2\eta^T P\Xi(\tilde{L}) \\ &= \eta^T\big[(A-KC)^T P + P(A-KC)\big]\eta + 2\eta^T P\big(\tfrac{\partial\Xi}{\partial\tilde{L}}\big)\tilde{L} \\ &\le c_1 V_1 + c_2\sqrt{V_1 V_2} \end{aligned} \tag{19}$$

Where $c_1$and c_2 are coefficients which depend on the set of P, K and Γ_L. Let us now derive the time derivative of V_2. One obtains

$$\begin{aligned} \dot{V}_2 &= \dot{\tilde{L}}^T\Gamma_L^{-1}\tilde{L} + \tilde{L}^T\Gamma_L^{-1}\dot{\tilde{L}} \\ &= (y-\hat{y})^T G^T\tilde{L} + \tilde{L}^T G(y-\hat{y}) \\ &= 2\tilde{L}^T G C\tilde{x} \\ &\le 2\tilde{L}^T G C(\eta + \Theta\tilde{L}) \\ &= 2\tilde{L}^T G C\Theta\tilde{L} + 2\tilde{L}^T G C\eta \\ &\le c_3 V_2 + c_4\sqrt{V_1 V_2} \end{aligned} \tag{20}$$

Where c_3 and c_4 are coefficients which depend on the set of G and Θ. Hence, using (19) and (20), one obtains

$$\begin{aligned} \dot{V} &= \dot{V}_1 + \dot{V}_2 \\ &\le c_1 V_1 + c_2\sqrt{V_1 V_2} + c_3 V_2 + c_4\sqrt{V_1 V_2} \\ &= c_1 V_1 + c_3 V_2 + (c_2 + c_4)\sqrt{V_1 V_2} \end{aligned} \tag{21}$$

By setting appropriate c_1, c_2, c_3 and c_4, one derives that $\dot{V}$ is negative semi-definite. From the Lyapunov candidate function V, one can obtain

$$\begin{aligned} &\min(\lambda_{\min}(P),\lambda_{\min}(\Gamma_L^{-1}))\Big(\big\|\eta\big\|^2 + \big\|\tilde{L}\big\|^2\Big) \\ &\le V \le \max(\lambda_{\max}(P),\lambda_{\max}(\Gamma_L^{-1}))(V_1+V_2)\Big(\big\|\eta\big\|^2 + \big\|\tilde{L}\big\|^2\Big) \end{aligned} \tag{22}$$

consequently V is lower bounded. Synthesizing (21) and (22), based on Barbalat's lemma for stability analysis, it is concluded that the system (14) is an adaptive observer with exponential convergence. This ends the proof. □

C. Capacitance estimation for the output capacitor

If a fault for the capacitor is detected and isolated by the fault diagnosis observer, a capacitance estimation observer is triggered to estimate the accurate value of capacitance offset. As can be seen from (5), the capacitance variance only affects the matrix A and the lower equation of (5). For the sake of convenience, we can denote only the faulty subsystem as

$$\dot{U}_o = \frac{I_L}{C+\Delta C} - \frac{U_o}{R(C+\Delta C)} \tag{23}$$

Also, it can be represented in state-space format as follows:

$$\begin{aligned} \dot{x} &= a(C+\Delta C)\,x + b(C+\Delta C,R)\,u \\ y &= x \end{aligned} \tag{24}$$

where $x = U_o$, $u = I_L$, $a = -\frac{1}{RC}$, and $b = \frac{1}{C}$. So, the observer is designed as follows:

$$\begin{aligned} \dot{\hat{x}} &= A\big(C+\Delta\hat{C}\big)\hat{x} + B\big(C+\Delta\hat{C},R\big)u + K_{22}\big(y-\hat{y}\big) \\ \hat{y} &= \hat{x} \\ \Delta\dot{\hat{C}} &= \mu_C\big(y-\hat{y}\big) \end{aligned} \tag{25}$$

Where K_{22} is the elements of the matrix K, denoting the coefficient errors as follows:

$$\begin{aligned} a(C+\Delta C) &= a(C) + \tilde{a}(C+\Delta C) \\ b(C+\Delta C,R) &= b(C,R) + \tilde{b}(C+\Delta C,R) \end{aligned} \tag{26}$$

Then, if the estimation error can be denoted as $e_C(t) = \Delta C - \Delta\hat{C}$, the error dynamics is described by

$$\begin{aligned} \dot{e}(t) &= (a - K_{22}c)\,e(t) + F \\ F &= [-\tilde{a}(C+\Delta C)]\,\hat{x} - \tilde{b}(C+\Delta C, R)\,u \end{aligned} \tag{27}$$

A further theorem on how to get μ_C above is given as follows:

Theorem 4. *With the observer gain K in theorem 1 and a defined constant $Q_C > 0$, and positive parameter γ_C , if there exist two constant P_C and G_C satisfying:*

$$\begin{aligned} 2P_C(a - K_{22}) + \gamma_C P_C &= -Q_C \\ P_C B_C &= {G_C}^T \end{aligned} \tag{28}$$

Then the observer given in (12) *with the adaptive fault estimation law is stated as follows:*

$$\Delta\hat{C} = \tau_C \int \left(y - \hat{y}\right) \tag{29}$$

can lead to $\lim_{t\to\infty} e(t) = 0$ *and* $\lim_{t\to\infty} e_C(t) = 0$, *where* τ_C *is a positive constant value.*

Proof. the proof of Theorem 4 is similar to Theorem 3 and can be seen as a corollary and single-dimension case of ODE. This ends the proof. □

IV. Simulation Results

In order to verify the feasibility and effectiveness of the proposed observers,we designed a DC-DC converter with parameters listed in TABLE I for verification. Firstly, different component faults are injected into the buck converter, and the corresponding FDD results are analyzed. Secondly, the variable inductance fault and capacitance fault are respectively injected into the buck converter, and the inductance and capacitance estimation results are analyzed. Finally, a mixed fault scenario with parameters drifts of both inductance and capacitance is performed, and the corresponding parameter estimation results are discussed.

TABLE I
Simulation Buck Converter Parameters.

$R[\Omega]$	7	$V_{in}[V]$	20
$L[H]$	5×10^{-4}	$V_{out}[V]$	8
$C[F]$	5.8×10^{-5}	$i_{out}[A]$	8/7
$F[kHz]$	10	PWM Duty Ratio	0.4

A. Fault diagnosis result

The fault diagnosis observer is firstly used to detect and isolate the different component faults based on the residuals. In order to make the residual signals clear enough to discriminate between different faults, we set the FD observer gain K as

$$K = \begin{bmatrix} 1 & 0 \\ 0 & 1 \end{bmatrix} \tag{30}$$

The state variables, estimate and residuals of the buck converter in fault-free mode can be seen in Fig. 5. As can be seen from Fig. 5, the inductor current displays as a small ripple because of the PWM controlling effect, while the output voltage is more stable because of the output filter's smoothing. The observer estimation can track the system states very closely because of the feedback gainąfs effect. Also, the residuals converge to zero very quickly, which is useful to detect faults.

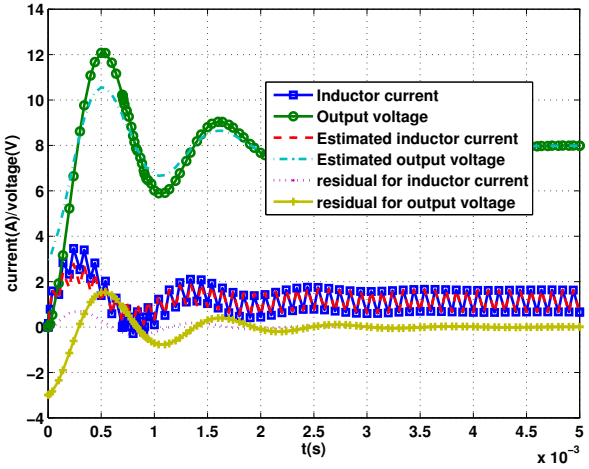

Fig. 5. States of the buck converter,observer estimation and residuals in fault-free mode.

The residuals under different fault modes can be seen in Fig. 6. An open-circuit fault and a short-circuit fault are respectively injected at the instant 0.05 s. A constant capacitance variation from C to 2C is injected at the instant 0.03 s; also a constant inductance variation from L to $2L$ is injected at the instant 0.03 s. From the residuals subjected to different faults, we can see that the residuals are no longer zero at the instants when faults occur, and also the fault signatures off different components are different. Fig. 6(a) and Fig. 6(b) depict the residuals under switch faults. It is clear that open-circuit fault and short-circuit fault have different effects on the residuals. Fig. 6(c) and Fig. 6(d) depict the residuals under capacitor and inductor faults. It is obviously clear that capacitor fault and inductor fault have different effects on the residuals. The residuals are also simple to identify from the residuals under the switch Q faults.

B. Condition parameter estimation result

Once the FD observer detects and isolates the faulty components, the corresponding parameter estimation observer is triggered to estimate the condition parameter. In order to verify the tracking performance subjected to faults with different temporary signatures, we consider two types of fault: constant parameter drafting and time-varying parameter drafting. The capacitance estimations under constant parameter drafting and time-varying parameter drafting are shown in Fig. 7, the inductance estimations are

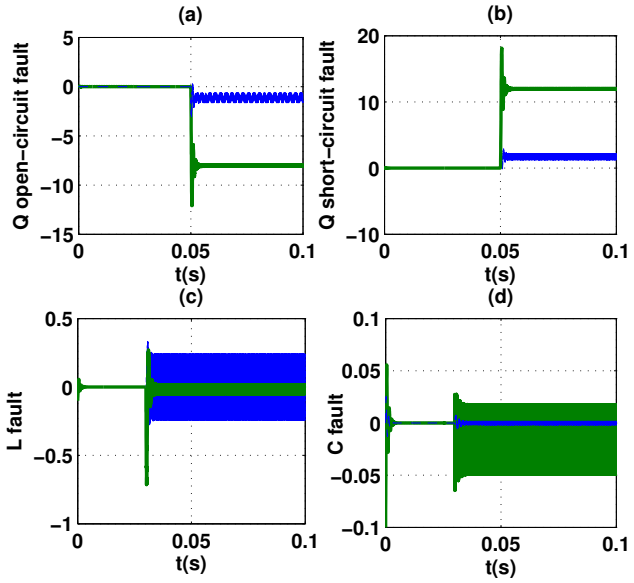

Fig. 6. Residuals under different fault modes(solid green line: FD observer error of inductor current[A], blue dash line: FD observer error of output voltage[V]).

shown in Fig. 8. Also, a compound scenario comprising of both capacitance and inductance parameter drafting are considered for verification, which is shown in Fig. 9.

1) Capacitance estimation: The capacitance estimation observer parameters are designed as follows:

$$\begin{aligned} \tau_C &= 5 \\ k_{22} &= 1 \end{aligned} \tag{31}$$

The constant parameter drafting of capacitance from C to 2C occurs at the instant 0.03 s. As can be seen from Fig. 7(a), the observer estimation can track the parameter drafting at 0.03 s very quickly and matches the target value closely.

The time-varying parameter drafting of capacitance begins at the instant 0.03 s. As can be seen from Fig. 7(b), the observer estimation can track the parameter drafting at 0.03 s very quickly keep to the target value closely.

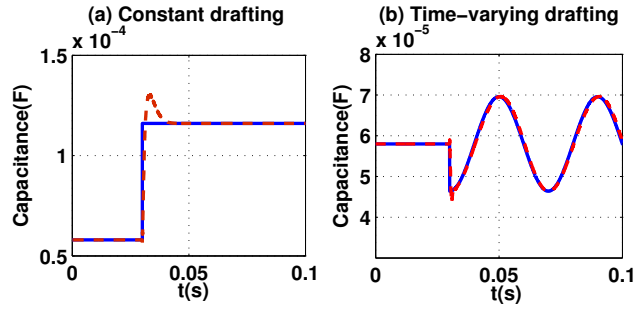

Fig. 7. Condition parameter drafting estimation for capacitance(solid line: real capacitance, dash line: estimation value).

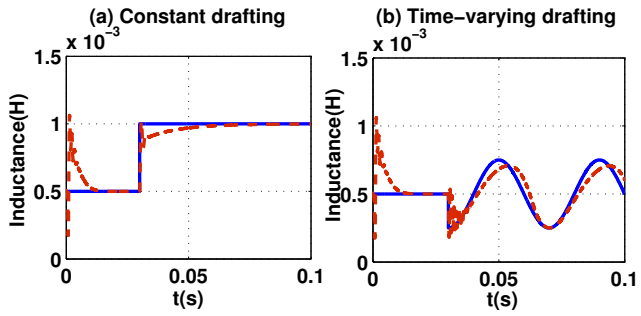

Fig. 8. Condition parameter drafting estimation for inductance(solid line: real inductance, dash line: estimation value).

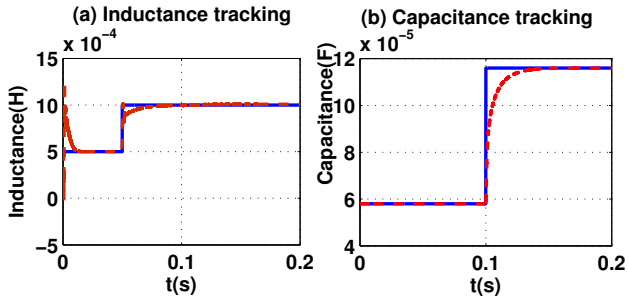

Fig. 9. Compound fault estimation results(solid line: real value, dash line: estimation value).

2) Inductance estimation: The inductance estimation observer parameters are designed as follows:

$$\begin{aligned} K &= \begin{bmatrix} 1 & 0 \\ 0 & 1 \end{bmatrix} \\ \mu_L &= [\,\text{-2.5}\ \ \text{-1.09}\,] \\ \tau_L &= [\,\text{-0.0001}\ \ \text{-0.000001}\,] \end{aligned} \tag{32}$$

The constant parameter drafting of inductance from L to 2L occurs at the instant 0.03 s. As can be seen from Fig. 8(a), the observer estimation tracks the parameter drafting at 0.03 s very quickly and keep to the target value closely.

The time-varying parameter drafting of inductance begins at the instant 0.03 s. As can be seen from Fig. 8(b), the observer estimation can tracks the parameter drafting at 0.03 s very quickly keeping to the target value closely.

3) Compound fault estimation: In order to verify the compound fault estimation performance, a compound fault is considered. Firstly, the inductance parameter drafting from L to 2L occurs at the instant 0.05 s. Secondly, the capacitance parameter drafting from C to 2C occurs at the instant 0.1 s. As can be seen from Fig. 9, the corresponding estimation observer can track the parameter drafting quickly and closely. There is almost no interference between the componentsąŕ failure to the observer estimation.

V. Experiment Validation for Conventional Buck Converters

A. Experiment setup

In order to validate the effectiveness of the proposed method, a buck converter experiment platform is setup for demonstration. In this platform, a conventional and inexpensive DC-DC buck converter module (shown at the bottom-right of Fig. 10 is utilized and modified for demonstration. The DC-DC buck converter employs an HRD05003 IC module as the controller to generate PWM signals and driver switch-on and switch-off of the circuit. The main electrical parameters of the buck converter are listed in Table. II. For test convenience, the inductor and capacitor in the original buck converter circuit are moved to a dedicated self-made circuit for test (shown in Fig. 11), and an LEM current sensor is embedded and additional power circuit is deployed in the circuit loop to acquire the inductor current. As can be seen from Fig. 11, four node signals (Input voltage, PWM modulated Voltage, inductor current, output voltage) are observed and recorded by the NI Compact RIO measurement device and the oscilloscope. Fig. 12 displays a snapshot of the recorded node signals. As can be seen from the waveforms displayed in Fig. 12, the converter operates at a frequency 301.397 kHz, which follows well with the rated switching frequency 300 kHz. Due to on-off effects of the MOSFETs, the measured output voltage and inductor current comprise some disturbance and offset error but the output voltage is almost stable and acceptable for applications.

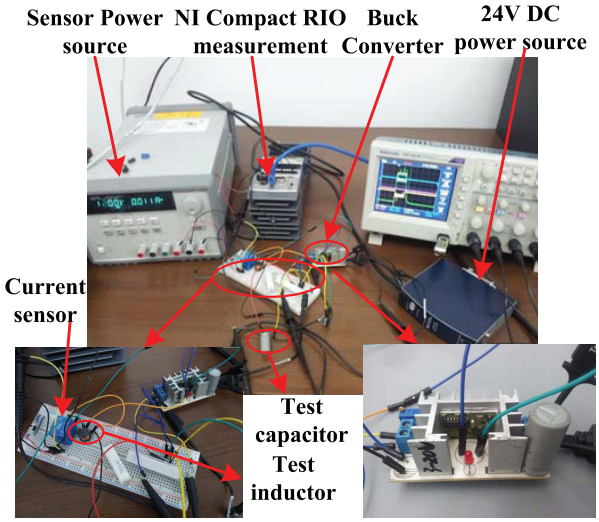

Fig. 10. Experimental Setup of the buck converter circuit.

B. Inductance estimation

A snapshot of recorded signals for inductance estimation is shown in Fig. 13. The three-node signals including

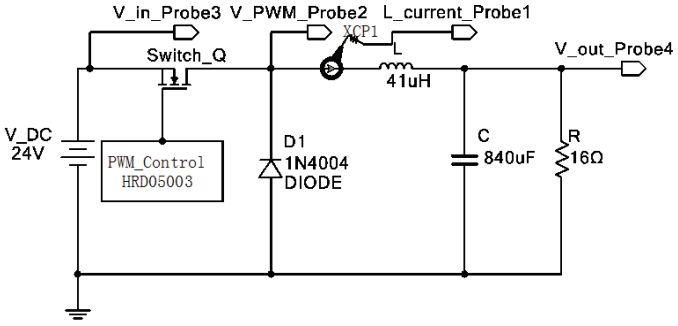

Fig. 11. Probe observing Nodes in the converter circuit.

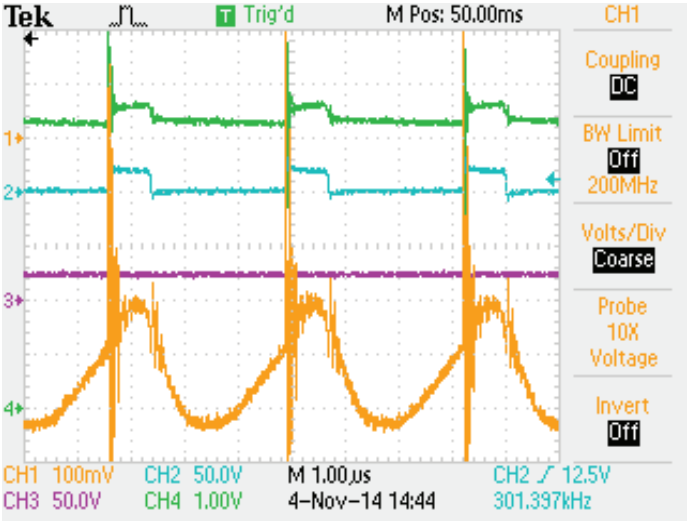

Fig. 12. A snapshot of recorded signals.

PWM modulated Voltage, inductor current, output voltage, are utilized for signal processing based on the model observer approach. For comparison and validation, the inductor (with ferrite core) is taken from the setup circuit and tested separately by an LCR meter, which is shown in left side of Fig. 14 while the inductor is shown in the right side of Fig. 14. As can be seen from Fig. 14, The LCR meter indicates that the actual inductance is 41.36 uH, while the rated inductance printed at the top of the inductor is 27 uH (270 means 27*100=27 uH) . The difference between the actual value and rated value is normal because of fabrication factors; it is also the reason accurate inductance validation and estimation is usually needed in such cases.

According to the observer theory in Section 3.2, the inductor current and output voltage is the state variables of the observer. The comparison between real states and

TABLE II
Experimental Buck Converter Parameters.

$R[\Omega]$	16	$V_{in}[V]$	24
$L[H]$	4.1×10^{-5}	$V_{out}[V]$	5.3
$C[F]$	8.4×10^{-4}	$i_{out}[A]$	5.3/16
$F[kHz]$	300	PWM Duty Ratio	0.25

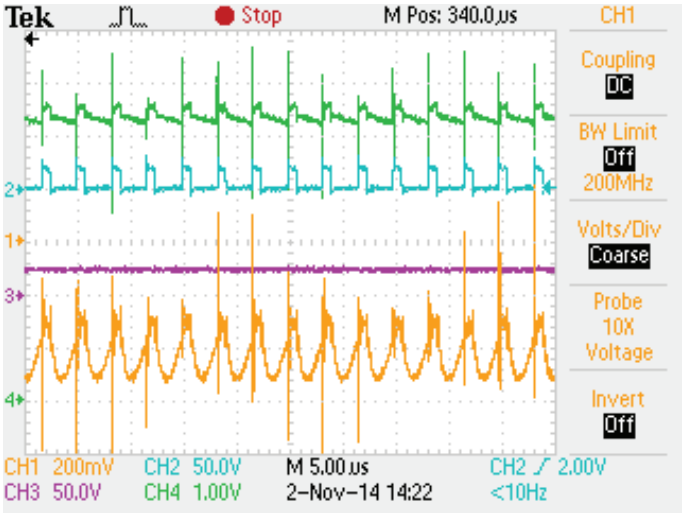

Fig. 13. A snapshot of recorded signals for inductance estimation.

Fig. 14. Tested inductor and test value by LCR meter.

observer estimated states is shown in Fig. 15. As can be from Fig. 15, the observer state estimations track well with its real states at a fast convergence speed, while the observer residuals are also bounded and stable, which means that the feedback adjustment and adaptive law of the observer works well. The inductance estimation results are shown in Fig. 16. In order to test the robustness of estimation performance, different estimation results subjected to three initial values (70 uH, 60 uH and 50 uH) are shown together for comparison. As can be seen from Fig. 16, the estimation converge into the actual value at a fast speed and the error due to measurement disturbance is bonded, which means the proposed observer still works well to estimate the real inductance in real experiment scenarios.

Comment 1: It is difficult to re-implement the parameter drafting or degradation for components in hardware because generally component degradation is a slow process. In order to validate the effectiveness and robustness of the proposed condition parameter estimation scheme under various scenarios, setting various initial values for the estimation is generally an acceptable alternative approach.

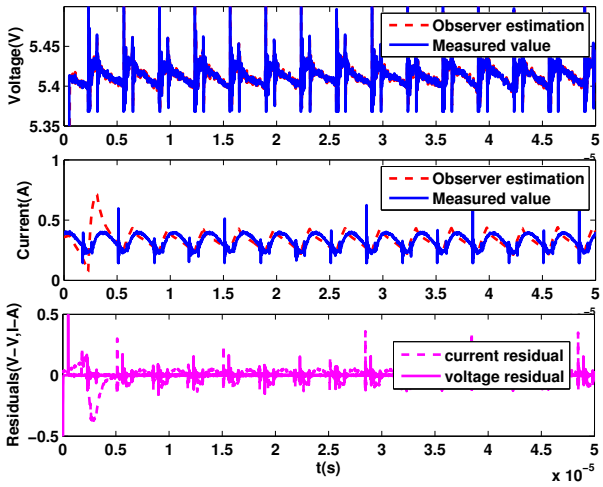

Fig. 15. Observer estimated states and residuals.

For this reason we set three different initial values for validation instead of changing the estimated component parameters, to match the simulation scenarios.

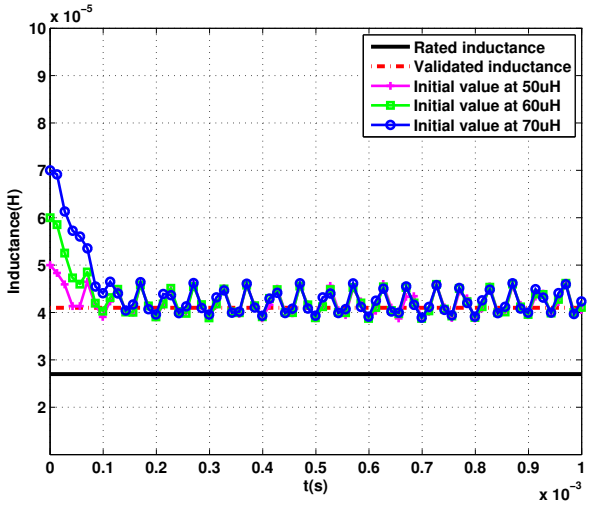

Fig. 16. Inductance estimation results.

C. Capacitance estimation

A snapshot of recorded signals for inductance estimation is shown in Fig. 17. Because different capacitance at the stable stage of the Buck converter operation has weak effects at node signal variations of the Buck converter, the node signal waveforms acquired at the start stage will be better and feasible for engineering implementation. Hence, the node signal waveforms at the start stage are utilized for capacitance estimation. As can be seen from Fig. 17, the output voltage and inductor current converge into a stable value because the capacitor is charged progressively.

For comparison and validation, the capacitor is taken from the setup circuit and tested separately by an LCR

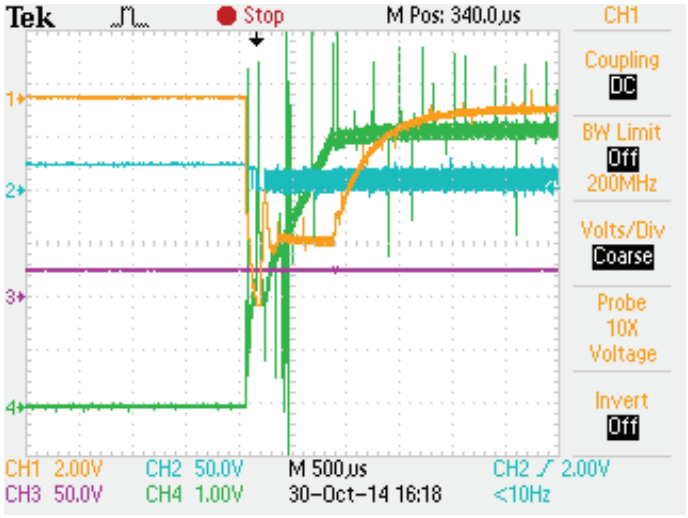

Fig. 17. A snapshot of recorded signals for capacitance estimation.

meter, which is shown in left side of Fig. 18 while the capacitor is shown in the right side of Fig. 18. As can be seen from Fig. 18, The LCR meter indicates that the actual capacitance is 839.2 uF, while the rated capacitance printed at the skin of the capacitor is 1000 uF. As can be drawn from literature about capacitor reliability, the difference between the actual value and rated value of capacitance is generally normal and caused by variable factors such as manufacturing tolerances, fabrication, aging and degradation.

Fig. 18. Tested capacitor and test value by LCR meter.

According to the observer theory in Section 3.3, the output voltage is the only state variable of the observer. Because the internal resistance of the real capacitor, the measured voltage is different from the capacitor voltage, a filtered and compensated output voltage is utilized for capacitance estimation. The comparison between real state, filtered value and observer estimation is shown in Fig. 19. As can be from Fig. 19, the observer state estimation tracks well with the filtered value at a fast convergence speed which means that the feedback adjustment and adaptive law of the observer work well.

The capacitance estimation results are shown in Fig. 20.

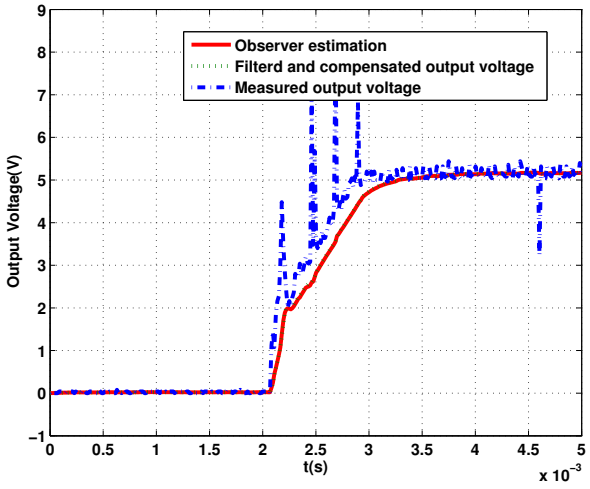

Fig. 19. Comparison among real value, filtered value and observer estimation.

In order to test the robustness of estimation performance, different estimation results subjected to three initial values (600 uF, 700 uF and 800 uF) are shown together for comparison. As can be seen from Fig. 20, the estimation converges into the actual value at a fast speed and the error due to measurement disturbance is bounded, which means the proposed observer still works well to estimate the real capacitance in real experiment scenarios .

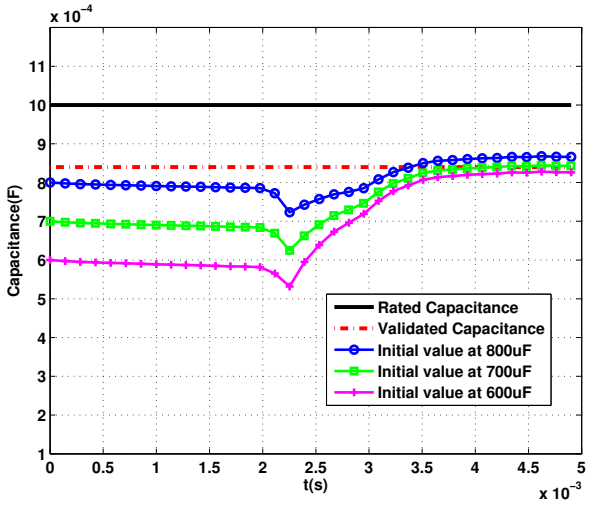

Fig. 20. Capacitance estimation results.

VI. Validation for Buck Converter under PV MPPT Control

Due to its penetration in Maximum Power Point Tracking (MPPT) applications, Buck converters generally work as a MPPT power charger for batteries or solar panel optimizers. In order to validate the proposed scheme under MPPT control for Buck converters and check its applicability for variable power inputs such as PV panels,

we design a typical solar panel DC-DC conversion topology to test the MPPT control and the proposed condition parameter estimation scheme. Fig. 21 depicts the topology of a Buck converter under MPPT control. In Fig. 21, due to time-varying and insolation-sensitive characteristics of PV panels, the input capacitor C1 is normally important and necessary to regulate the PV panel output voltage, but not an essential component for general Buck converters depicted in Fig. 2. In this section, we can see the input capacitor C1 as an external component and only consider to monitor the capacitor C2.

The parameters for the PV panel, buck converter and MPPT controller in the proposed topology are listed Table .III.

A. Simulation results

Based on the parameters defined as Table .III. The Buck DC-DC conversion variables under MPPT can be seen in Fig. 22. Fig. 22(a) and(c) show how the PV panel output voltage and current is controlled to track the value at the MPP point, the PV panel output starts from open-circuit voltage and keeps stable at the MPP voltage(17.2 V) while the PV panel current starts from zero current and keeps stable at the MPP current(4.95 A). Fig. 22(b) depicts the converter output voltage for load and Fig. 22(d) depicts the inductor current, both of the two variables have high-frequency ripples, making the condition parameter estimation more challenging. From the two variables, we can see that the Buck converter works and output power is stable under MPPT control. Due to its inherit drawback of the P&O algorithm, the PV panel output voltage and current will keep oscillating in a small range, but it is acceptable for Buck converter DC power output.

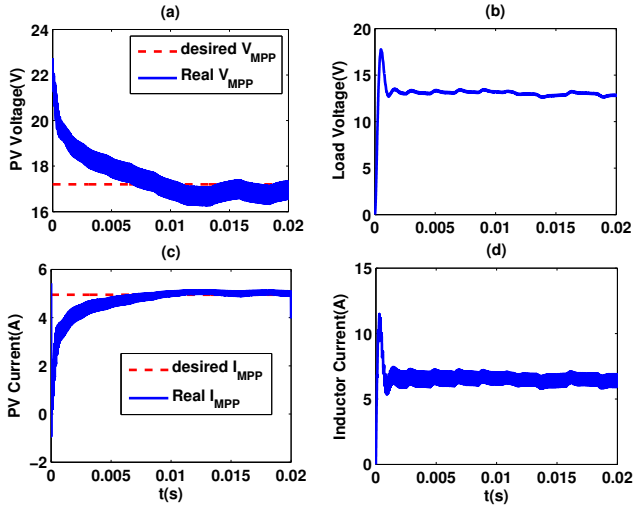

Fig. 22. Input and Output of MPPT Buck converter.

Fig. 23 depicts the condition parameter estimation results under MPPT with constant insolation. From Fig. 23(a) we can see that the P&O MPPT algorithm works very fast to track the MPP at 17.2*4.95=85 W. Fig. 23(b) depicts that the duty ratio converges into a bonded boundary around 0.23-0.25, which means that the DC-DC conversion is precisely executed by the buck converter. The capacitance and inductance estimation results are shown in Fig. 23(c) and (d). From the tracking results, we can see the proposed condition parameter estimation scheme can track the real capacitance and inductance although the power input (PV panel output) for Buck converter is not constant.

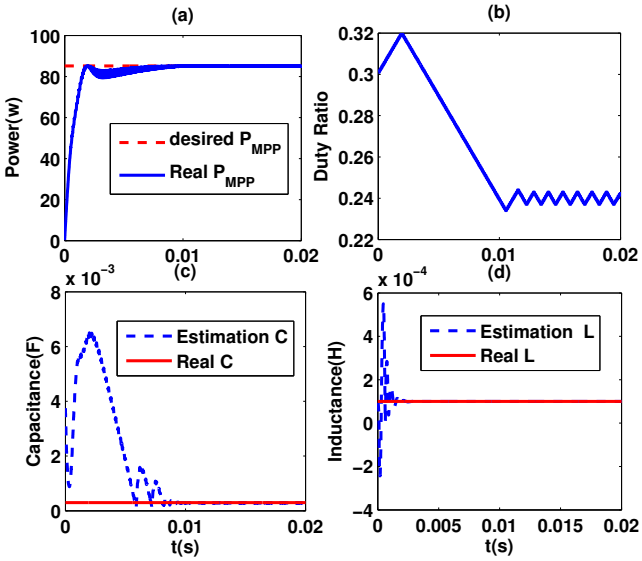

Fig. 23. Condition Parameter Estimation Results under MPPT with constant insolation.

Fig. 24 depicts the condition parameter estimation results under MPPT with time-varying insolation, which varies from 1000 to 800 at the instant 0.002 s. From Fig. 24(a) we can see that the P&O MPPT algorithms work very fast to track two-stage MPPs at 85 W and 65 W individually. Fig. 24(b) depicts that the duty ratio converges into two stable range due to the insolation variation. The capacitance and inductance estimation results are shown in Fig. 24(c) and (d). From the tracking results, we can see the proposed condition parameter estimation scheme can track the real capacitance and inductance although the buck converter output voltage is oscillating and the insolation is time-varying.

B. Experiment results

In order to validate the effectiveness of the proposed scheme under real-time control and real-world power analogue signal measurement, a real-time controller-based prototype MPPT buck converter system is built at a dSPACE/ControlDesk-based lab setup, which is shown in Fig. 25 and 26. As can be seen from Fig. 26, both the MPPT Buck conversion topology and condition estimation scheme are executed in the dSPACE real-time target system, the two physical units interact with real-world analogue acquiring signals, which is connected by corresponding analogue signal cables and connectors. The

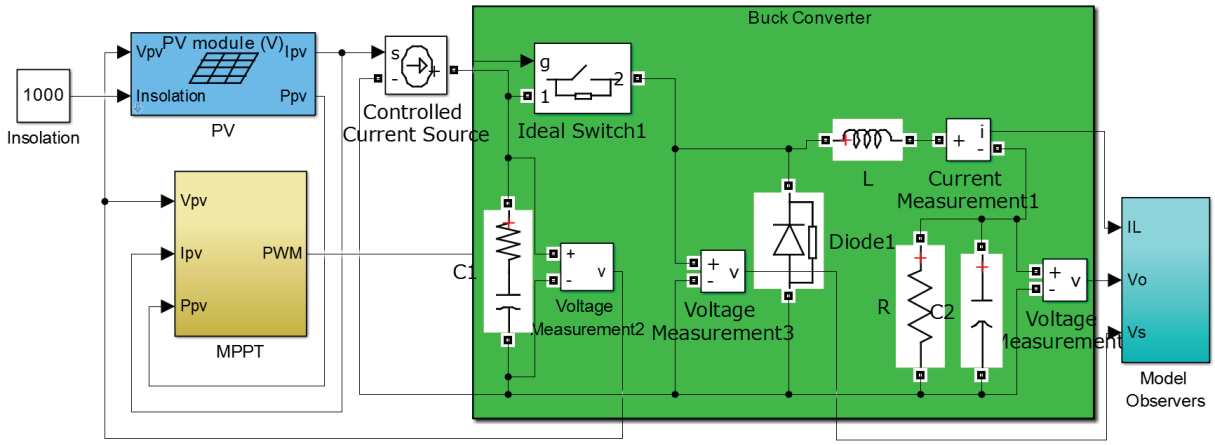

Fig. 21. Designed topology of a buck converter under MPPT control.

TABLE III
DESIGNED MPPT BUCK CONVERTER PARAMETERS.

$V_{oc}[V]$	22.2	$T[°C]$	25
$I_{sc}[A]$	5.45	$R_p[\Omega]$	98.7192
$V_{max}[V]$	17.2	$R_s[\Omega]$	0.4716
$I_{max}[A]$	4.95	$Insolation[w/m^2]$	1000
$R[\Omega]$	2	$Frequency[Hz]$	10000
$L[H]$	3×10^{-4}	$PWM\ \ Duty\ \ Ratio$	1000
$C_2[F]$	1×10^{-4}	$C_1[F]$	3×10^{-4}
$Duty\ \ Ratio\ \ Step$	0.001	$MPPT\ \ algorithm$	$Peturb\ \ and\ \ Observe$
$Initial\ \ Value\ \ of\ \ DR$	0.5	$Sampling\ \ Rate$	10000

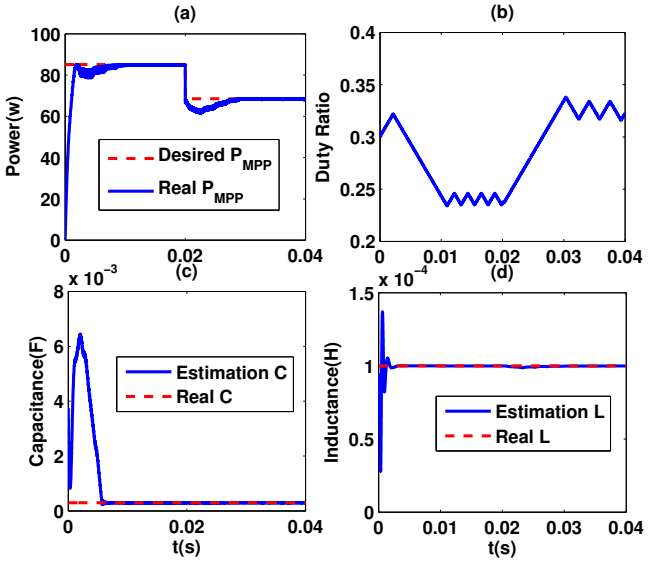

Fig. 24. Condition Parameter Estimation Results under MPPT with time-varying insolation.

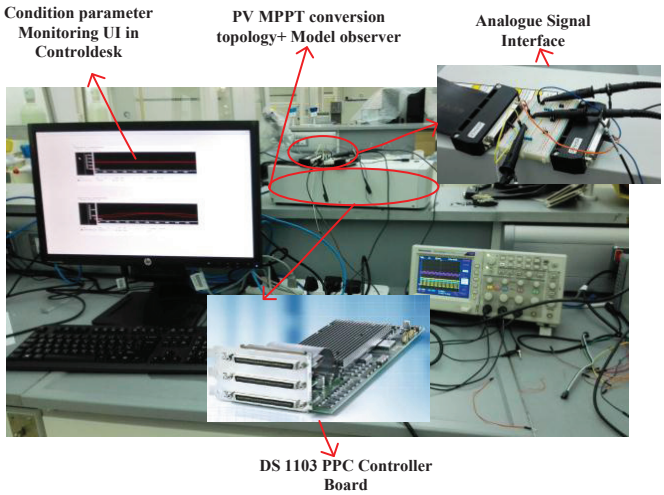

Fig. 25. dSPACE/Controldesk-based lab setup for MPPT buck converter system.

interaction signals including output voltage, inductor current, and diode voltage are monitored by a scope, which is shown in Fig. 25.

The real-time condition parameter estimation experiment results can be seen in Fig. 27-30. As can be seen from Fig. 27-29, the waveform and dynamics match the corresponding signals of the real-world buck converter in Section V. The condition parameters are monitored in real-time by ControlDesk platform that runs on the host PC. As can be seen from Fig. 30 which is a screenshot from ControlDesk, the capacitance and inductance are estimated and monitored in real-time with high accuracy.

VII. CONCLUSION

This paper proposes a condition parameter estimation scheme based on model observers for Buck converters.

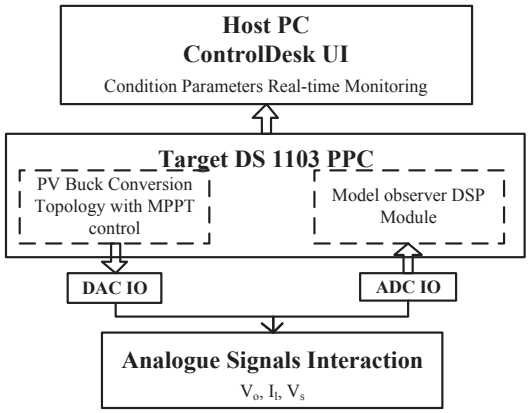

Fig. 26. Real-time controller-based prototype diagram for MPPT buck converter system.

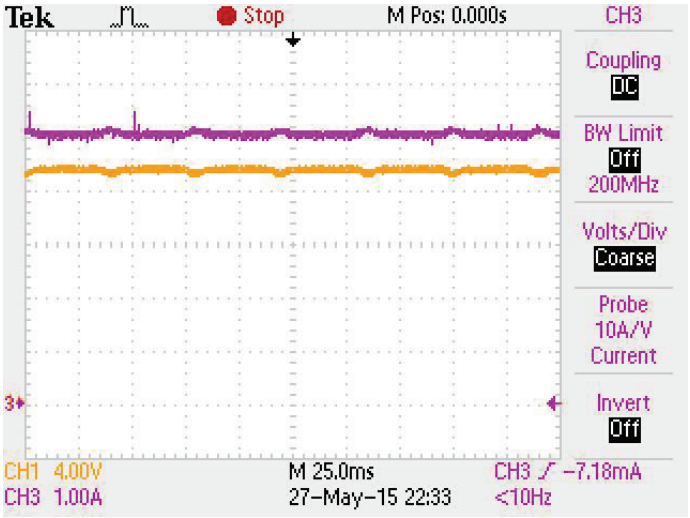

Fig. 27. Solar panel output voltage and current.

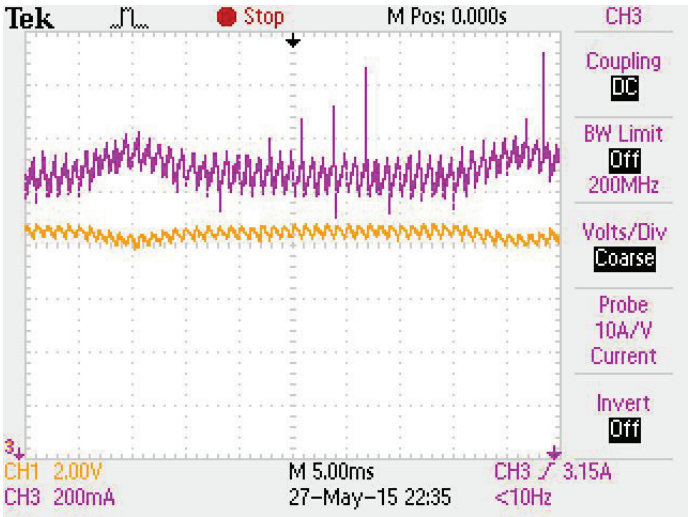

Fig. 28. Enlarged picture of Solar panel output voltage and current.

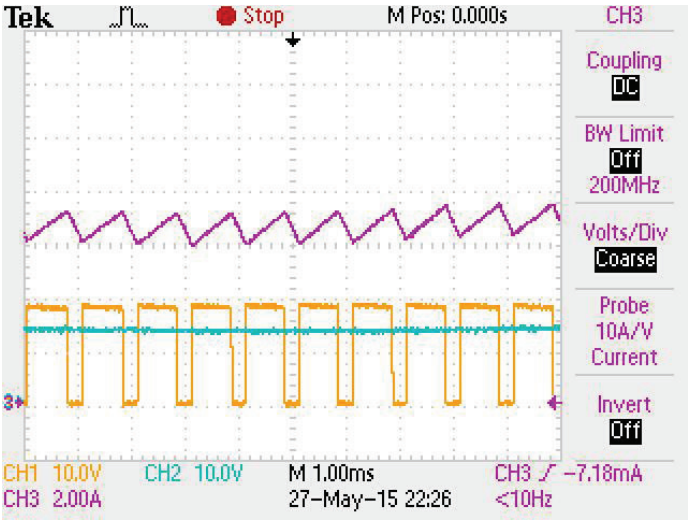

Fig. 29. Real-time Monitoring Variables used for Condition parameter estimation.

Fig. 30. Real-time Monitoring UI for Condition Parameters in ControlDesk.

Two novel observers in the CPE scheme are proposed and theoretically proved. With the FD observer, Fault detection and isolation for components can be availed based on the residual signals. With the corresponding adaptive parameter estimation observers, an accurate estimation of parameter drafting can be addressed for condition monitoring and reliability analysis. Real-world Buck converter experiments for conventional DC-DC conversion and PV MPPT control are set up to validate the effectiveness of the proposed model observer method. A further study of general online monitoring approach on separate capacitors in any circuit typologies is on-going. Future work will consider more components such as IGBT and more types of converters applied in PV systems such as boost converters and other inverters.

ACKNOWLEDGMENT

The authors would like to thank xxxxx for xxxxx.

REFERENCES

[1] S. V. Dhople, A. Davoudi, A. D. Domínguez-García, and P. L. Chapman, "A unified approach to reliability assessment of multiphase dc–dc converters in photovoltaic energy conversion systems," *Power Electronics, IEEE Transactions on*, vol. 27, no. 2, pp. 739–751, 2012.

[2] S. V. Dhople, A. Davoudi, P. L. Chapman, and A. D. Domínguez-García, "Reliability assessment of fault-tolerant dc-dc converters for photovoltaic applications," in *Energy Conversion Congress and Exposition, 2009. ECCE 2009. IEEE*. IEEE, 2009, pp. 2271–2276.

[3] S. V. Dhople and A. D. Domínguez-García, "Estimation of photovoltaic system reliability and performance metrics," *Power Systems, IEEE Transactions on*, vol. 27, no. 1, pp. 554–563, 2012.

[4] H. Al-Sheikh, O. Bennouna, G. Hoblos, and N. Moubayed, "Condition monitoring of bidirectional dc-dc converter for hybrid electric vehicles," in *Control and Automation (MED), 2014 22nd Mediterranean Conference of*. IEEE, 2014, pp. 97–102.

[5] H.-K. Cho, S.-S. Kwak, and S.-H. Lee, "Fault diagnosis algorithm based on switching function for boost converters," *International Journal of Electronics*, no. ahead-of-print, pp. 1–15, 2014.

[6] M. Shahbazi, E. Jamshidpour, P. Poure, S. Saadate, and M. Zolghadri, "Open- and short-circuit switch fault diagnosis for nonisolated dc/dc converters using field programmable gate array," *Industrial Electronics, IEEE Transactions on*, vol. 60, no. 9, pp. 4136–4146, Sept 2013.

[7] P. S. Das and K.-H. Kim, "Real-time multiple open-switch fault diagnosis in three-phase ac/dc pwm converter for pmsg based grid-connected wind power generation system." *International Journal of Control & Automation*, vol. 7, no. 9, 2014.

[8] D. Divan, R. Moghe, and A. Prasai, "Power electronics at the grid edge: The key to unlocking value from the smart grid," *Power Electronics Magazine, IEEE*, vol. 1, no. 4, pp. 16–22, 2014.

[9] M. Aragues Penalba, O. Gomis-Bellmunt, and M. Martins, "Coordinated control for an offshore wind power plant to provide fault ride through capability," *Sustainable Energy, IEEE Transactions on*, vol. 5, no. 4, pp. 1253–1261, 2014.

[10] J. T. Bialasiewicz, "Renewable energy systems with photovoltaic power generators: Operation and modeling," *Industrial Electronics, IEEE Transactions on*, vol. 55, no. 7, pp. 2752–2758, 2008.

[11] D. Foito, V. F. Pires, F. Amaral, and J. Martins, "A neuro-fuzzy based system for fault detection and diagnosis of 3-phase pfc rectifier," in *Power Electronics and Motion Control Conference and Exposition (PEMC), 2014 16th International*. IEEE, 2014, pp. 71–76.

[12] H. Henao, G. Capolino, M. Fernandez-Cabanas, F. Filippetti, C. Bruzzese, E. Strangas, R. Pusca, J. Estima, M. Riera-Guasp, and S. Hedayati-Kia, "Trends in fault diagnosis for electrical machines: A review of diagnostic techniques," *Industrial Electronics Magazine, IEEE*, vol. 8, no. 2, pp. 31–42, 2014.

[13] B. Ilhem, B. Amar, A. Lebaroud, and R. Fares, "Automatic fault diagnosis of fault tolerant power converter for switched reluctance motor based on time-frequency technique," in *Power Electronics and Motion Control Conference and Exposition (PEMC), 2014 16th International*. IEEE, 2014, pp. 1234–1240.

[14] E. Jamshidpour, M. Shahbazi, S. Saadate, P. Poure, and E. Gholipour, "Fpga based fault detection and fault tolerance operation in dc-dc converters," in *Power Electronics, Electrical Drives, Automation and Motion (SPEEDAM), 2014 International Symposium on*. IEEE, 2014, pp. 37–42.

[15] J. Lee and K. Lee, "An open-switch fault detection method and tolerance controls based on svm in a grid-connected t-type rectifier with unity power factor," *Industrial Electronics, IEEE Transactions on*, vol. 61, no. 12, pp. 7092–7104, 2014.

[16] C. Yao, Z. Zhao, Y. Chen, X. Zhao, Z. Li, Y. Wang, Z. Zhou, and G. Wei, "Transformer winding deformation diagnostic system using online high frequency signal injection by capacitive coupling," *Dielectrics and Electrical Insulation, IEEE Transactions on*, vol. 21, no. 4, pp. 1486–1492, 2014.

[17] A. Mora, P. Lezana, and J. Juliet, "Control scheme for an induction motor fed by a cascade multicell converter under internal fault," *Industrial Electronics, IEEE Transactions on*, vol. 61, no. 11, pp. 5948–5955, 2014.

[18] H. Wang, K. Ma, and F. Blaabjerg, "Design for reliability of power electronic systems," in *IECON 2012-38th Annual Conference on IEEE Industrial Electronics Society*. IEEE, 2012, pp. 33–44.

[19] F. Blaabjerg, K. Ma, and D. Zhou, "Power electronics and reliability in renewable energy systems," in *Industrial Electronics (ISIE), 2012 IEEE International Symposium on*. IEEE, 2012, pp. 19–30.

[20] R. Wang, Z. Zhang, X. Kavousianos, Y. Tsiatouhas, and K. Chakrabarty, "Built-in self-test, diagnosis, and repair of multimode power switches," *Computer-Aided Design of Integrated Circuits and Systems, IEEE Transactions on*, vol. 33, no. 8, pp. 1231–1244, 2014.

[21] P. Lezana, J. Pou, T. A. Meynard, J. Rodriguez, S. Ceballos, and F. Richardeau, "Survey on fault operation on multilevel inverters," *Industrial Electronics, IEEE Transactions on*, vol. 57, no. 7, pp. 2207–2218, 2010.

[22] Y. Song and B. Wang, "Survey on reliability of power electronic systems," *Power Electronics, IEEE Transactions on*, vol. 28, no. 1, pp. 591–604, 2013.

[23] X. Yu and A. M. Khambadkone, "Reliability analysis and cost optimization of parallel-inverter system," *Industrial Electronics, IEEE Transactions on*, vol. 59, no. 10, pp. 3881–3889, 2012.

[24] H. Zhang and L. Xu, "Diagnostic system for current-carrying fault: Modeling, precaution, and prediction," *IEEE transactions on power delivery*, vol. 29, no. 3, pp. 1318–1325, 2014.

[25] E. Ribeiro, A. Cardoso, and C. Boccaletti, "Fault diagnosis in unidirectional non-isolated dc-dc converters," in *Energy Conversion Congress and Exposition (ECCE), 2014 IEEE*. IEEE, 2014, pp. 1140–1145.

[26] Y. Xiong, "Modeling and analysis of power mosfets for high frequency dc-dc converters," Ph.D. dissertation, University of Central Florida, Orlando, Florida, May 2008. [Online]. Available: http://purl.fcla.edu/fcla/etd/CFE0002278

[27] Y. Xiong, X. Cheng, Z. J. Shen, C. Mi, H. Wu, and V. K. Garg, "Prognostic and warning system for power-electronic modules in electric, hybrid electric, and fuel-cell vehicles," *Industrial Electronics, IEEE Transactions on*, vol. 55, no. 6, pp. 2268–2276, 2008.

[28] S. Khomfoi and L. M. Tolbert, "Fault diagnostic system for a multilevel inverter using a neural network," *Power Electronics, IEEE Transactions on*, vol. 22, no. 3, pp. 1062–1069, 2007.

[29] ——, "Fault diagnosis and reconfiguration for multilevel inverter drive using ai-based techniques," *Industrial Electronics, IEEE Transactions on*, vol. 54, no. 6, pp. 2954–2968, 2007.

[30] S. Yin, S. Ding, X. Xie, and H. Luo, "A review on basic data-driven approaches for industrial process monitoring," *IEEE Transactions on Industrial Electronics*, vol. 61, no. 11, pp. 6418–6428, 2014.

[31] V. Spinu, M. Dam, and M. Lazar, "Observer design for dc/dc power converters with bilinear averaged model," in *Analysis and Design of Hybrid Systems*, 2012, pp. 204–209.

[32] M. Alavi, M. Luo, D. Wang, and D. H. Zhang, "Fault diagnosis for power electronic inverters: A model-based approach," in *Diagnostics for Electric Machines, Power Electronics & Drives (SDEMPED), 2011 IEEE International Symposium on*. IEEE, 2011, pp. 221–228.

[33] X. Ding, J. Poon, I. Celanovic, and A. D. Dominguez-Garcia, "Fault detection and isolation filters for three-phase ac-dc power electronics systems," *Circuits and Systems I: Regular Papers, IEEE Transactions on*, vol. 60, no. 4, pp. 1038–1051, 2013.

[34] J. Poon, A. Genic, X. Ding, A. Dominguez-Garcia, and I. Celanovic, "A linear-switched observer for large-signal state estimation in power electronics," in *Power Electronics and Motion Control Conference (EPE/PEMC), 2012 15th International*. IEEE, 2012, pp. LS3b–3.

[35] K. T. Levin, E. M. Hope, and A. Domínguez-García, "Observer-based fault diagnosis of power electronics systems," in *Energy Conversion Congress and Exposition (ECCE), 2010 IEEE*. IEEE, 2010, pp. 4434–4440.

[36] N. Gonzalez-Fonseca, D. Leon-Morales, and J. Leyva-Ramos, "Observer-based controller for switch-mode dc-dc converters," in *Decision and Control, 2005 and 2005 European Control Conference. CDC-ECC'05. 44th IEEE Conference on*. IEEE, 2005, pp. 4773–4778.